On the flat representation for a particular class of port-Hamiltonian systems

I. Zafeiratou, I. Prodan, L. Lefèvre

Version of Record: https://www.sciencedirect.com/science/article/pii/S2405896320332468
Manuscript_c2e1b27ac8522bd284fc9fc111849eed

On the flat representation for a particular class of port-Hamiltonian systems

I. Zafeiratou * **I. Prodan** * **L. Lefèvre** *

* *Univ. Grenoble Alpes, Grenoble INP* ⋆*, LCIS, F-26000 Valence, France (e-mail: igyso.zafeiratou, ionela.prodan, laurent.lefevre@lcis.grenoble-inp.fr)*

Abstract: This paper pertains to the flat representation of a class of port-Hamiltonian (PH) systems and advocates the use of bicausality of Bond graphs for finding appropriate flat outputs. Systems which are differentially flat have several useful properties which can be exploited to generate, for example, optimal trajectories/profiles which ensure constraints satisfaction. For the special case of PH systems combining the power preserving property with the flatness properties leads to effective control strategies for multi-physical systems. Hence, the purpose of this paper is to explore the implications and features of a particular class of PH systems (which can be retrieved from a Bond Graph representation) in finding their flat output representation. We concentrate on the example of an electrical storage system of a DC microgrid to illustrate the proposed theory.

Keywords: Flatness, Bond graphs, Bicausality, Port-Hamiltonian systems, Electrical storage

1. INTRODUCTION

Differential flatness is a structural property of a class of nonlinear dynamical systems, i.e., all system variables (the states and inputs) are written in terms of a set of specific variables, the *flat outputs* (equal in number to the number of inputs), and their derivatives (Levine (2009)).

There is a wide range of works which employ differential flatness in their control approach. Many researchers use its properties in motion planning problems (Hervagault et al., 2019) in order to validate the system's dynamics under constraints and generate optimal profiles for velocity, forces and the like. Other works employ B-Splines parametrization of the flat outputs to ensure continuous-time constraints validation at the trajectory generation level Zafeiratou et al. (2018); Pham et al. (2015).

The idea of this paper is inspired by our recent works (Zafeiratou et al., 2018) where we propose a flatness-based hierarchical control for power balancing in a meshed DC microgrid. Firstly, through the PH formulation, the state-space representation of the microgrid system was explicitly and structurally described. Next, the differential flatness was employed to obtain the relations of the states and control inputs in function of the flat outputs. By using flatness combined with B-splines parametrization, we were able to generate optimal profiles for the current and voltage of the energy storage (ES) system while minimizing the electricity purchase from the external grid.

However, an important issue is the calculation of the flat outputs, especially in the case of a complex dynamics with multiple states and inputs. Franke and Robenack (2013) proposed an algorithm for calculating the flat outputs of nonlinear physical systems using illustrative examples. This algorithm was implemented in Zafeiratou et al. (2018) to find a possible flat output set for the ES PH system. Apart from the algorithm, another method has been studied in (Richard et al., 2002). It relies upon an important advantage of the PH systems according to which their state-space representations can be easily derived from their Bond graph representation. Therefore, through Bond graphs and a recently established notion called bicausality, the inverse dynamics of the PH systems will be studied and linked to their flat representations.

The contributions of this paper are: i) use of the bicausal Bond graphs to analyze the flat representation of the PH systems; ii) development of a method which provides directly the number of states and inputs that could be taken into account as possible flat outputs for the PH system; iii) analysis of the proposed technique over an electrical storage system.

2. BOND GRAPHS AND BICAUSALITY

Bond graph is a graph-oriented approach and builds upon the power-preserving interconnections amongst the elements of a physical system Karnopp et al. (2012). An important characteristic of the Bond graph is the causality property which indicates the dependence among the port elements [1] characterized by pairs of efforts e and flows f as in Fig. 1. Every element has different causality structure. In here, we will focus on the storage elements (capacitors and inductors) which define the states of the electrical systems mentioned below. There are two types of causalities, the integral and the differential causality.

Integral causality: The input is integrated to generate the output (see also Fig. 2a). For the capacitors we have

⋆ Institute of Engineering Univ. Grenoble Alpes

[1] For electrical systems, e is the voltage and f is the current.

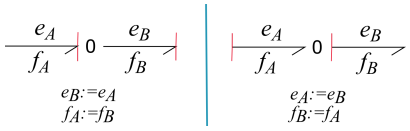

Fig. 1. Causality in the Bond graphs indicated in red.

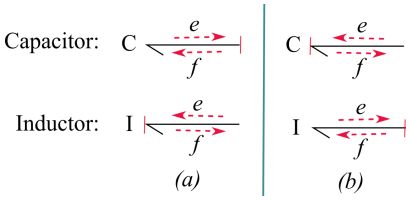

Fig. 2. (a) Integral causality of the storage elements. (b) Differential causality of the storage elements.

$e = \frac{1}{C}\int^t f\,dt$ and for the inductors $f = \frac{1}{I}\int^t e\,dt$ (where C is the capacitance and I is the inductance). Concerning the dissipative elements, R, they obey to a static constitutive law which provides only algebraic relations between the effort and flow, $e = f \cdot R$ and $f = \frac{e}{R}$. Fig. 3 depicts the causal Bond graph of the RLC circuit depicted on the left. The red dashed lines illustrate the power flow and the dependence among the port variables.

Differential causality: The input's time derivative equals to the ratio of the output (see also Fig. 2b). For the capacitors wa have $\frac{de}{dt} = \frac{f}{C}$ and for the inductors $\frac{df}{dt} = \frac{e}{I}$. Differential causality is used in the inverse Bond graphs, else called bicausal Bond graphs, as in Fig. 5.

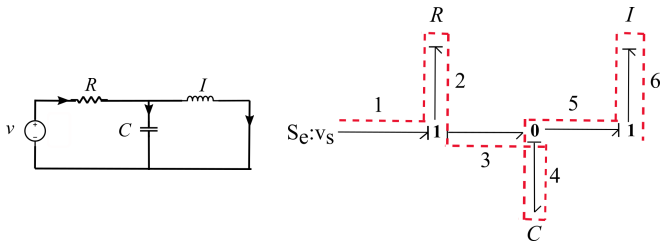

Fig. 3. Electrical RLC circuit and its causal Bond graph.

Bicausality: It is an extended version of causality which allows the interpretation of the inverse dynamics (Richard et al., 2002). In order to design a bicausal Bond graph, supplementary elements are taken into account which enable the decoupling of $e - f$ pairs and facilitate the calculation of further quantitative variables (Fig. 4). The SS (source-sensor) elements are added, which contain the inputs and the outputs of the system (e.g., the effort sources, S_e, the flow sources, S_f, the effort detectors, D_e , the flow detectors, D_f). The sources elements have specific assignment , which is the opposite assignment from the case of the causal Bond graph, indicating the inverse dynamics. Similarly, for the storing elements as in Fig. 2b(Ngwompo and Gawthrop, 1999).

Bicausality of a RLC circuit: The bicausal Bond graph of the RLC circuit is introduced in Fig. 5. From the bicausal Bond graph, the following relations are obtained from the 0 and 1 junctions (keep in mind that p is the magnetic flux

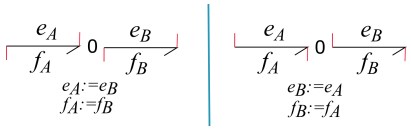

Fig. 4. Relation among the $e - f$ elements in the bicausal Bond graphs.

of the inductor and q is the charge of the capacitor) [2] :

$$\begin{aligned} &e_1 = e_3 + e_4, \\ &f_2 = f_3 = f_4, \; f_5 = C\frac{de_5}{dt} = \dot{q}, \; e_5 = \frac{1}{C}\int^t f_5 dt = \frac{q}{C}, \\ &e_4 = e_5 = e_6, \\ &f_4 = f_5 + f_6, \; e_7 = I\frac{df_7}{dt} = \dot{p}, \; f_7 = \frac{1}{I}\int^t e_7 dt = \frac{p}{I}, \\ &e_6 = e_7, \\ &f_6 = f_7, \qquad e_R = f_R R = (f_5 + f_6)R = (\dot{q} + \frac{p}{I})R. \end{aligned} \tag{1}$$

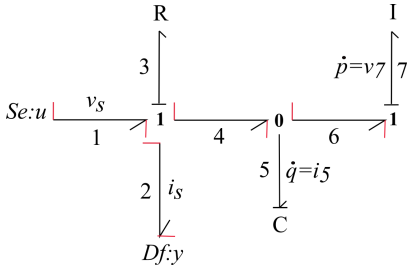

Fig. 5. Bicausal Bond graph of the electrical RLC circuit.

3. BICAUSALITY AND DIFFERENTIAL FLATNESS

Hereinafter, the connection between bicausality and differential flatness will be analyzed.

Taking into account the definition of differential flatness (see Levine (2009)), we show that the flatness property can be derived from the bicausal Bond graph representation of an electrical circuit detailed in Section 2.

Proposition 3.1. Let us consider the state vector $x(t) \in \mathbb{R}^2$ and inputs $u(t) \in \mathbb{R}$ derived by the bicausal Bond graph of the RLC circuit. The state and input resulted by the bicausal Bond graph is considered to be equivalent to the flat representation of the system (see Levine (2009)).

Proof: From (1), the states and inputs are derived for the bicausal Bond graph in Fig. 5:

$$p = If_7 = I(\dot{q} + \frac{p}{I} - \dot{q}), \tag{2a}$$

$$q = Ce_5 = C\dot{p}, \tag{2b}$$

$$u = v_s = (\dot{q} + \frac{p}{I})R + \dot{p}, \tag{2c}$$

where v_s is the input voltage supplied by the source. The state vector of the system is $x = [p\ q]^\top \in \mathbb{R}^{2\times 1}$ and the input vector is $u = v_s \in \mathbb{R}^{1\times 1}$. Regarding the relations above, (2a)-(2c), provided through the bicausal Bond graph, a physical representation is obtained similar to the flat representation of the system, considering the flat outputs in function of the states (see definition of flatness). According to Levine (2009), the number of flat outputs must be equal to the number of control inputs. The RLC system (2a-2c) has one control input, $u = v_s$. Therefore,

[2] Wherever it is straightforward implied by the text, we will discard the time dependence.

one flat output is necessary. Note that from the bicausal Bond graph (Fig. 5), we retrieve the state p and obtain (2a), which shows that p cannot be written in function of the other variables of the RLC circuit, the state q and the input v_s. Consequently, a straightforward choice is the state p as a possible flat output for the system, $z = p$. Therefore, we obtained a flat representation of the system through its bicausal Bond graph. □

4. FROM BICAUSAL BOND GRAPHS TO DIRAC STRUCTURES

In this section, we go further and analyze the connection between bicausal Bond graphs of electrical circuits and their PH formulation. Then going back, we can actually retrieve the flat representation of a PH system.

In general, PH systems are determined by the interconnections among the elements included in a physical system through a Dirac Structure (DS) (see definition in (van der Schaft et al., 2014)). The DS connects all the port variables together and obeys to the power conservation among the elements (van der Schaft et al., 2014).

Proposition 4.1. (Link between bicausal Bond graphs and Dirac structures): If the bicausal Bond graph admits a kernel representation (see definition in (van der Schaft et al., 2014)), then it is a Dirac structure, hence a PH system. As a consequence, in the case of the electrical circuits, the flat representation of their PH models can be analyzed through their bicausal Bond graphs.

Proof: The proof is given over a particular example of an ES system (see the circuit in Fig. 6) which includes the KiBaM battery [3] and the Split-Pi converter.

Let us represent in Fig. 7 the causal Bond graph of the KiBaM battery, part of the ES electrical circuit presented in Fig. 6. Its corresponding state-space representation in PH form derived by its causal Bond graph has been already presented in Zafeiratou et al. (2018). Developing, next, the inverse dynamics of the battery's system through its bicausal Bond graph (Fig. 8), we will derive the possible flat outputs of the battery.

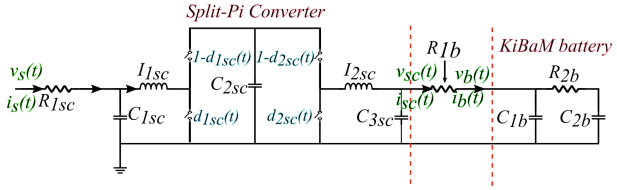

Fig. 6. Electrical circuit of the ES system composed by the Split-Pi converter and the KiBaM battery.

Fig. 8 presents the bicausal Bond graph of the battery composed by two storing elements, the capacitors C_{1b} and C_{2b} of the battery with their differential causalities, one effort source, S_e, which is the input (the voltage of the Split-Pi converter, v_{sc}), and one flow detector, D_f, which is the output (the current of the Split-Pi converter, i_{sc}). Therefore, the state and input of the system are give:

[3] KiBaM stands for the kinetic battery model.

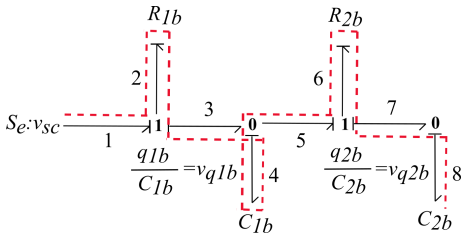

Fig. 7. Causal Bond graph of the KiBaM battery.

$$q_{1b} = \dot{q}_{2b} R_{2b} C_{1b} + \frac{C_{1b}}{C_{2b}} q_{2b}, \tag{3a}$$

$$q_{2b} = v_{sc} C_{2b} - \dot{q}_{1b} R_{1b} C_{2b} - \dot{q}_{2b} R_{1b} C_{2b} - \dot{q}_{2b} R_{2b} C_{2b}, \tag{3b}$$

$$v_{sc} = \dot{q}_{1b} R_{1b} + \dot{q}_{2b} R_{1b} + \dot{q}_{2b} R_{2b} + \frac{q_{2b}}{C_{2b}}. \tag{3c}$$

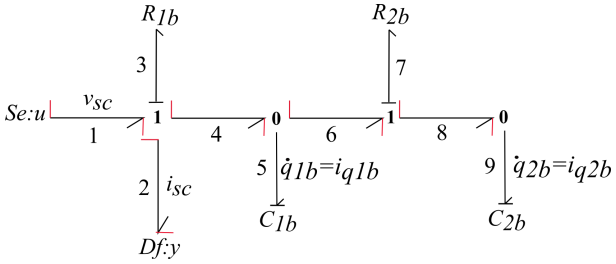

Fig. 8. Bicausal bond graph of the KiBaM battery.

According to Proposition 4.1, if the aforementioned system can be written in kernel representation, it composes a DS. Therefore, the kernel representation of the bicausal Bond graph in Fig. 8 is presented below:

$$\underbrace{\begin{bmatrix} 1 & -1 & 0 & 1 & 0 \\ -1 & 0 & 1 & 0 & 1 \\ 0 & 0 & 0 & 0 & 0 \\ 0 & 0 & 0 & 0 & 0 \\ 0 & 0 & 0 & 0 & 0 \end{bmatrix}}_{E} \underbrace{\begin{bmatrix} v_{q_{1b}} \\ v_{q_{2b}} \\ v_{R_{1b}} \\ v_{R_{2b}} \\ v_{sc} \end{bmatrix}}_{e} + \underbrace{\begin{bmatrix} 0 & 0 & 0 & 0 & 0 \\ 0 & 0 & 0 & 0 & 0 \\ 1 & 1 & 0 & 0 & 1 \\ 0 & 0 & 1 & 0 & -1 \\ 0 & 1 & 0 & 1 & 0 \end{bmatrix}}_{F} \underbrace{\begin{bmatrix} i_{q_{1b}} \\ i_{q_{2b}} \\ i_{R_{1b}} \\ i_{R_{2b}} \\ i_s \end{bmatrix}}_{f} = \begin{bmatrix} 0 \\ 0 \\ 0 \\ 0 \\ 0 \end{bmatrix}, \tag{4}$$

Hence, the bicausal Bond graph of the battery is a PH system. Indeed, by isolating the derivatives of the states on the left side in (3a)-(3c), we conclude to the PH state-space representation presented in Zafeiratou et al. (2018). Afterwards, all the possible relations among the efforts and flows, derived from the 0 and 1 junctions of the bicausal Bond graph (Fig. 8), are presented below:

$$\begin{bmatrix} q_{1b} \\ q_{1b} \\ q_{2b} \\ q_{2b} \\ v_{sc} \\ v_{sc} \end{bmatrix} = \begin{bmatrix} 0 & 0 & \frac{C_{1b}}{C_{2b}} & R_{2b}C_{1b} & 0 \\ 0 & -R_{1b}C_{1b} & 0 & -R_{1b}C_{1b} & C_{1b} \\ 0 & 0 & 1 & 0 & 0 \\ 0 & 0 & 1 & 0 & 0 \\ 0 & R_{1b} & \frac{1}{C_{2b}} & R_{1b}+R_{2b} & 0 \\ 0 & 0 & 0 & 0 & 1 \end{bmatrix} \begin{bmatrix} q_{1b} \\ \dot{q}_{1b} \\ q_{2b} \\ \dot{q}_{2b} \\ v_{sc} \end{bmatrix}. \tag{5}$$

From the latter matrix representation, in the left part the states and the inputs are illustrated, which, regarding the definition of flatness, can be written in function of the flat outputs and their derivatives. Since we have one control input, v_{sc}, we expect only one flat output (Levine, 2009). Furthermore, taking into account that the flat output can be written in function of the states, from (5) we can assume that the only possible flat output for the battery's system

is $z = q_{2b}$. This conclusion comes from the fact that it is the only state not written in function of the other states or their derivatives. To look more carefully at the result, we separate the matrices, extracting the circuit parameters, C_{1b}, C_{2b}, and the dissipation, R_{1b}, R_{2b}:

$$\begin{bmatrix} q_{1b} \\ \frac{q_{1b}}{C_{1b}} \\ \frac{q_{2b}}{C_{2b}} \\ \frac{q_{2b}}{C_{2b}} \\ u_s \\ u_s \end{bmatrix} = \left(\underbrace{\begin{bmatrix} 0&0&1&0&0 \\ 0&0&0&0&1 \\ 0&0&1&0&0 \\ 0&0&1&0&0 \\ 0&0&1&0&0 \\ 0&0&0&0&1 \end{bmatrix}}_{V} + \underbrace{\begin{bmatrix} 0 & 0 & 0 & R_{2b} & 0 \\ 0 & -R_{1b} & 0 & -R_{1b} & 0 \\ 0 & 0 & 0 & 0 & 0 \\ 0 & 0 & 0 & 0 & 0 \\ 0 & R_{1b} & 0 & R_{1b}+R_{2b} & 0 \\ 0 & 0 & 0 & 0 & 0 \end{bmatrix}}_{W} \right) \cdot \left[\frac{q_{1b}}{C_{1b}} \ \dot{q}_{1b} \ \frac{q_{2b}}{C_{2b}} \ \dot{q}_{2b} \ v_{sc} \right]^\top . \tag{6a}$$

Therefore, from matrix V we can derive the states and control inputs which are structurally required for the flat representation. The state q_{2b} is included, in function of which q_{1b} and v_{sc} can be derived (third column of matrix V). We notice also that in the last row of matrix V the control input v_{sc} appears. In W matrix, the dissipative elements are presented and are involved only with the derivatives of the states, which are not taken into consideration in the flat outputs selection. The flat representation of the battery is written below from (3a)-(3c):

$$q_{1b} = R_{2b}C_{1b}\dot{z} + \frac{C_{1b}}{C_{2b}}z, \tag{7a}$$

$$q_{2b} = z, \tag{7b}$$

$$v_{sc} = R_{2b}R_{1b}C_{1b}\ddot{z} + (R_{1b}\frac{C_{1b}}{C_{2b}} + R_{1b} + R_{2b})\dot{z} + \frac{1}{C_{2b}}z. \tag{7c}$$

Following the same steps, we continue with the Split-Pi converter. Firstly, its PH state-space representation is considered (see Fig. 7) as already presented in Zafeiratou et al. (2018). As aforementioned, since we have four control inputs at this case, we have to find four flat outputs. Developing the inverse dynamics of the system through its bicausal Bond graph, we will generate the four states or inputs which can be considered as flat outputs.

$$\begin{bmatrix} p_{1sc} \\ p_{1sc} \\ p_{2sc} \\ p_{2sc} \\ q_{1sc} \\ q_{1sc} \\ q_{2sc} \\ q_{3sc} \\ q_{3sc} \\ q_{3sc} \\ v_s \\ i_b \end{bmatrix}^\top = \begin{bmatrix} 1&0&0&0&0&0&0&0&0&0&0&0&0 \\ 0&0&0&0&-\frac{I_{1sc}}{C_{1sc}R_{1sc}}&-I_{1sc}&0&0&0&\frac{I_{1sc}}{R_{1sc}}&0&0&0 \\ 0&0&1&0&0&0&0&0&0&0&0&0&0 \\ 0&0&0&0&0&0&0&0&I_{2sc}&0&I_{2sc}&0&0 \\ 0&0&0&0&1&0&0&0&0&0&0&0&0 \\ 0&C_{1sc}&0&0&0&0&\frac{C_{1sc}}{C_{2sc}}&0&0&0&0&-C_{1sc}&0 \\ 0&0&0&0&0&0&1&0&0&0&0&0&0 \\ 0&0&0&0&0&0&0&1&0&0&0&0&0 \\ 0&0&0&-C_{3sc}&0&0&\frac{C_{3sc}}{C_{2sc}}&0&0&0&0&0&-C_{3sc} \\ 0&0&0&0&0&0&0&0&0&0&C_{3sc}R&0&0 \\ \frac{R_{1sc}}{I_{1sc}}&0&0&0&\frac{1}{C_{1sc}}&R_{1sc}&0&0&0&0&0&0&0 \\ 0&0&0&0&0&0&0&\frac{1}{C_{1sc}R}&0&0&0&0&0 \end{bmatrix} \begin{bmatrix} p_{1sc} \\ \dot{p}_{1sc} \\ p_{2sc} \\ \dot{p}_{2sc} \\ q_{1sc} \\ \dot{q}_{1sc} \\ q_{2sc} \\ q_{3sc} \\ \dot{q}_{3sc} \\ v_s \\ i_b \\ d_{1sc} \\ d_{2sc} \end{bmatrix}^\top \tag{8}$$

Fig. 10 presents the bicausal Bond graph of the Split-Pi converter, composed by five storing elements, the capacitors C_{1sc}, C_{2sc}, C_{3sc} and the inductors I_{1sc}, I_{2sc} with their differential causalities, one effort source, S_e, and the resistor R which contain the inputs (the voltage of the source, v_s, and the current of the resistor R, i_R), one flow detector, D_f, which is the first output (current of the source, i_s) and one effort detector, D_e, which is the second output (voltage of the resistor R) of the system. Furthermore, the duty cycles, d_{1sc} and d_{2sc}, correspond to the activity of the switches, Sw_{1sc}, Sw_{2sc}, Sw_{3sc}, Sw_{4sc}. Therefore, the states are derived below:

$$p_{1sc} = I_{1sc}\left(\frac{u_s}{R_{1sc}} - \frac{q_{1sc}}{C_{1sc}R_{1sc}} - \dot{q}_{1sc}\right), \tag{9a}$$

$$p_{2sc} = I_{2sc}\left[\dot{q}_{3sc} + i_R\right], \tag{9b}$$

$$q_{1sc} = C_{1sc}\left[\dot{p}_{1sc} + \frac{q_{2sc}}{C_{2sc}}(1 - d_{1sc})\right], \tag{9c}$$

$$q_{2sc} = q_{2sc}, \tag{9d}$$

$$q_{3sc} = C_{3sc}\left[\frac{q_{2sc}}{C_{2sc}}(1 - d_{2sc}) - \dot{p}_{2sc}\right]. \tag{9e}$$

Moreover, the control inputs can be deduced also in function of the states and their derivatives from the bicausal Bond graph as follows:

$$v_s = \left(\frac{p_{1sc}}{I_{1sc}} + \frac{q_{1sc}}{C_{1sc}R_{1sc}} + \dot{q}_{1sc}\right)R_{1sc}, \tag{10a}$$

$$i_R = \frac{q_{3sc}}{C_{3sc}R}, \tag{10b}$$

$$d_{1sc} = \frac{C_{2sc}}{q_{2sc}}\left(\dot{p}_{1sc} - \frac{q_{1sc}}{C_{1sc}} + \frac{q_{2sc}}{C_{2sc}}\right), \tag{10c}$$

$$d_{2sc} = \frac{C_{2sc}}{q_{2sc}}\left(-\dot{p}_{2sc} + \frac{q_{2sc}}{C_{2sc}} - \frac{q_{3sc}}{C_{3sc}}\right). \tag{10d}$$

Next, the kernel representation of the bicausal Bond graph of the Split-Pi converter is presented, which proves that it composes a DS:

$$\underbrace{\begin{bmatrix} -1&0&-1&1-d_{1sc}&0&0&0&0 \\ 0&1&0&1-d_{2sc}&-1&0&0&0 \\ 0&0&0&0&0&0&0&0 \\ 0&0&0&0&0&0&0&0 \\ 0&0&0&0&0&0&0&0 \\ 0&0&-1&0&0&-1&0&1 \\ 0&0&0&0&-1&0&-1&0 \\ 0&0&0&0&0&0&0&0 \end{bmatrix}}_{E} \underbrace{\begin{bmatrix} e_{p_{1sc}} \\ e_{p_{2sc}} \\ e_{q_{1sc}} \\ e_{q_{2sc}} \\ e_{q_{3sc}} \\ e_{R_{1sc}} \\ e_R \\ v_s \end{bmatrix}}_{e} + \tag{11a}$$

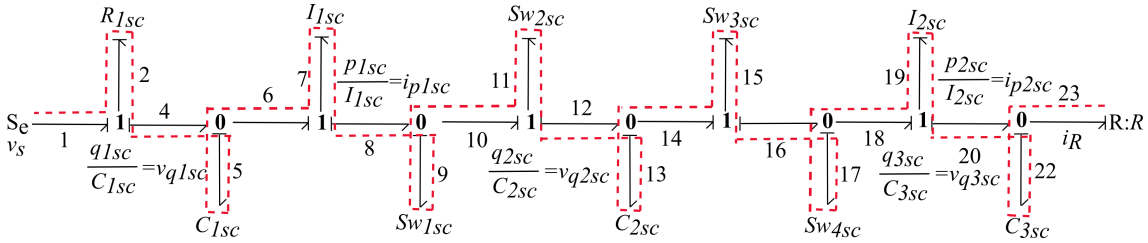

Fig. 9. Causal bond graph of the Split-Pi converter.

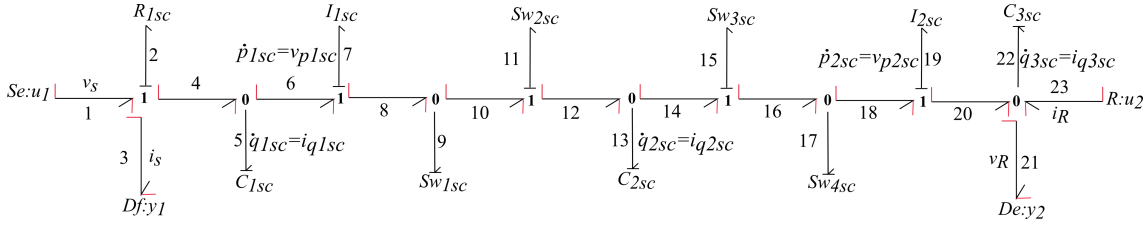

Fig. 10. Bicausal bond graph of the Split-Pi converter.

$$+\underbrace{\begin{bmatrix} 0 & 0 & 0\,0 & 0 & 0\,0\,0 \\ 0 & 0 & 0\,0 & 0 & 0\,0\,0 \\ -1 & 0 & 1\,0 & 0 & 0\,0\,1 \\ 1-d_{1sc} & -(1-d_{2sc}) & 0\,1 & 0 & 0\,0\,0 \\ 0 & -1 & 0\,0 & -1 & 0\,1\,0 \\ 0 & 0 & 0\,0 & 0 & 0\,0\,0 \\ 0 & 0 & 0\,0 & 0 & 0\,0\,0 \\ 0 & 0 & 0\,0 & 0 & 1\,0\,1 \end{bmatrix}}_{F} \underbrace{\begin{bmatrix} f_{p_{1sc}} \\ f_{p_{2sc}} \\ f_{q_{1sc}} \\ f_{q_{2sc}} \\ f_{q_{3sc}} \\ f_{R_{1sc}} \\ f_R \\ i_s \end{bmatrix}}_{f} = \begin{bmatrix} 0 \\ 0 \\ 0 \\ 0 \\ 0 \\ 0 \\ 0 \\ 0 \end{bmatrix},$$

Hence, the bicausal Bond graph of the Split-Pi converter is also a PH system. By placing the state derivatives on the left side in (9a)-(9e) (considering also the control inputs in (10a)-(10d)) leads to the primary PH state-space representation as in Zafeiratou et al. (2018).

Subsequently, all the relations among the flow and the effort variables from the 0 and 1 junctions (Fig. 10) are introduced below in (8). At this point, four additional relations are obtained for the states p_{1sc}, p_{2sc} and q_{2sc} concerning the duty cycles, d_{1sc} and d_{2sc}, of the converter:

$$\frac{p_{1sc}}{I_{1sc}} d_{1sc} = \frac{p_{1sc}}{I_{1sc}} - \dot{q}_{2sc} - \frac{p_{2sc}}{I_{2sc}}(1-d_{2sc}), \tag{12a}$$

$$\frac{p_{2sc}}{I_{2sc}} d_{2sc} = \frac{p_{2sc}}{I_{2sc}} - \dot{q}_{2sc} - \frac{p_{1sc}}{I_{1sc}}(1-d_{1sc}), \tag{12b}$$

$$\frac{q_{2sc}}{C_{2sc}} d_{1sc} = \frac{q_{2sc}}{C_{2sc}} - \frac{q_{1sc}}{C_{1sc}} + \dot{p}_{1sc}, \tag{12c}$$

$$\frac{q_{2sc}}{C_{2sc}} d_{2sc} = \frac{q_{2sc}}{C_{2sc}} - \frac{q_{3sc}}{C_{3sc}} - \dot{p}_{2sc}. \tag{12d}$$

These four equations will be also considered in the analysis of the flat outputs. During the operation of the converter the states p_{1sc}, p_{2sc}, q_{2sc} are different from 0. Contrariwise, the duty cycles, d_{1sc} and d_{2sc}, can be equal to 0. Therefore, the duty cycles cannot be placed in the denominator's position in the fractions appearing in (12a)-(12d) and cannot be included in the flat outputs selection.

The circuit's parameters and the dissipative elements are divided into two matrices as in (6a), hence (8) becomes:

$$\begin{bmatrix} p_{1sc} & \frac{p_{1sc}}{I_{1sc}} & p_{2sc} & \frac{p_{2sc}}{I_{2sc}} & q_{1sc} & \frac{q_{1sc}}{C_{1sc}} & q_{2sc} & q_{3sc} & \frac{q_{3sc}}{C_{3sc}} & \frac{q_{3sc}}{C_{3sc}} \\ v_s & i_b \end{bmatrix}^\top = (V+W) \begin{bmatrix} p_{1sc} & \dot{p}_{1sc} & p_{2sc} & \dot{p}_{2sc} & q_{1sc} & \dot{q}_{1sc} & q_{2sc} \\ q_{3sc} & \dot{q}_{3sc} & v_s & i_b & d_{1sc} & d_{2sc} \end{bmatrix}^\top, \tag{13}$$

where matrices V and W are developed as before, extracting the dissipative elements and placing them in W.

From (8), we can assume that a possible set of flat outputs for the Split-Pi converter system contains the states p_{1sc}, p_{2sc}, q_{1sc}, q_{2sc}, q_{3sc}. Concerning the state q_{2sc}, it must be regarded as one of the flat outputs (seventh row of matrix V). Since it cannot be expressed in function of the other states and inputs, it is necessary for the flat representation. Additionally, because of (12a)-(12d), it is indispensable to consider the states p_{1sc}, p_{2sc}, q_{2sc} as part of the flat outputs since they are linked with the switching activity of the converter (12a-12d). Moreover, the d_{1sc} and d_{2sc} are given only from (12a)-(12d) and they cannot be taken into account. The control inputs, v_s and i_b, similarly cannot be taken into account, since they are written in function of the states and their derivatives, but not vice-versa.

To decide the proper set of flat outputs, we must consider that the number of flat outputs derivatives in the flat representation can influence the signal response and create oscillations. Thereupon, we need to select which states are appropriate from (13) and (8) (less derivatives create less deviations among the reference and the actual values), so that the less possible derivatives appear in the flat representation. If we look into (8), the state q_{1sc} is in function of more than one derivatives, while the state q_{3sc} can be replaced from an equation with no derivatives included. However, neither can be excluded and the decision on the appropriate flat output depends on the kind of problem to solve as referred below. Therefore, we conclude to the following possible flat outputs:

$$z_1 = [p_{1sc}\ p_{2sc}\ q_{2sc}\ q_{1sc}]^\top, \tag{14}$$

$$z_2 = [p_{1sc}\ p_{2sc}\ q_{2sc}\ q_{3sc}]^\top. \tag{15}$$

The flat representation of the Split-Pi converter can be written, substituting in (9a)-(9e) and (10a)-(10d), each one of (14) and (15).

In Fig. 12 and Fig. 11, the control inputs from (10a)-(10d) are written in function of the two sets of flat outputs (14-15) and, after implementing the Split-Pi model in Matlab/Simulink both in PH form and in flat representation, the simulation results are obtained. The reference values of the control inputs are considered as $v_s = 400\ V$, $d_{1sc} = 0.6$, $d_{2sc} = 0.4$ and i_b (the input current of the battery), which varies (blue line in the last simulation of Fig. 12 and Fig. 11). Analyzing the two figures, Fig. 12 and Fig. 11, we observe that with (14) we obtain more stable and less noise-affected results for v_s. Contrariwise, i_b signal contains more noise-affected data. In the duty cycles, slight disturbances appear for both cases. In general, both sets of flat outputs, (14) and (15), can be considered for the flat representation of the Split-Pi converter. The flat

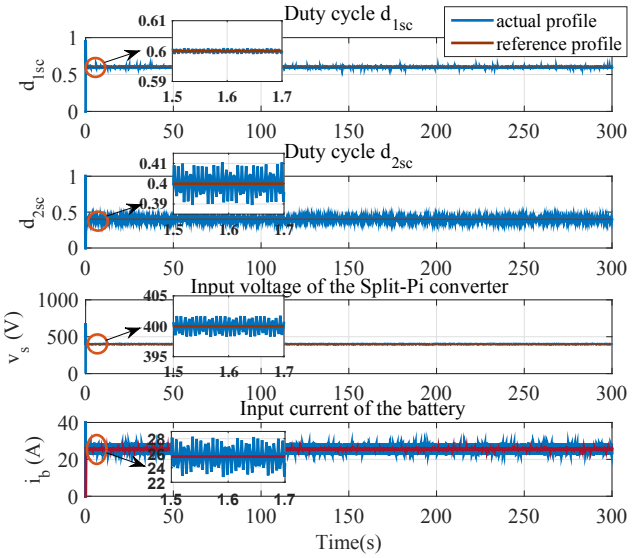

Fig. 11. Actual control inputs in function of the flat outputs set of (14). v_s, d_{1sc} and d_{1sc} are considered as constant in the reference PH system, while i_b varies.

representation in our case is further combined with the B-spline parametrization, strongly dependent on the number of derivatives included. To simplify the calculations (see also (10a)), the first set of flat outputs (14) would be the appropriate choice, because writing v_s in function of this set leads to a simpler differential equation with less derivatives.

5. CONCLUSION

The concept of bicausality and bicausal Bond graphs was presented. We attempted to link bicausality and Dirac structure of port-Hamiltonian systems through kernel representation. Every possible relations among the states and the control inputs were found from their bicausal Bond graphs. The idea was to find a method which provides the possible states, candidates for the flat representation of the PH systems. This method will be further extended for other port-Hamitonian physical systems.

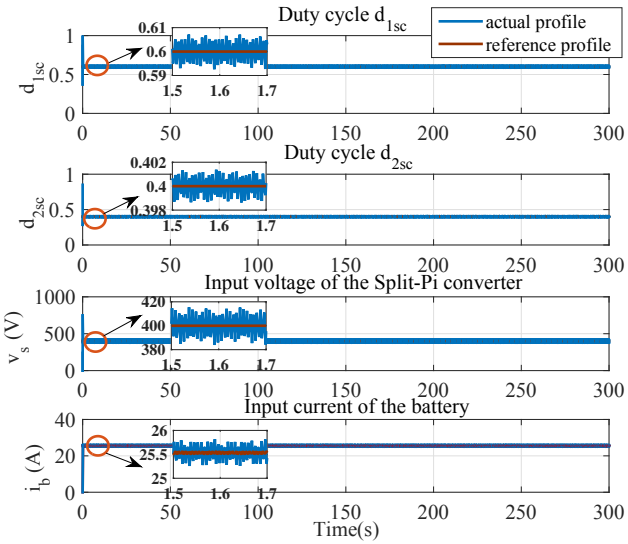

Fig. 12. Control inputs in function of the second set of flat outputs of (15). v_s, d_{1sc} and d_{1sc} and i_b have the same values as in the previous simulations (Fig. 11).

ACKNOWLEDGEMENTS

This work is funded by the French National Research Agency within the framework of the project ANR-15-CE05-004-02 $C^3\mu$.

REFERENCES

Franke, M. and Robenack, K. (2013). On the computation of flat outputs for nonlinear control systems. In *Control Conference (ECC), 2013 European*, 167–172. IEEE.

Hervagault, Y., Prodan, I., and Lefèvre, L. (2019). Motion planning for usvs with communication guarantees: an experimental setup. In *2019 18th European Control Conference (ECC)*, 3984–3989. IEEE.

Karnopp, D.C., Margolis, D.L., and Rosenberg, R.C. (2012). *System dynamics: modeling, simulation, and control of mechatronic systems*. John Wiley & Sons.

Levine, J. (2009). *Analysis and control of nonlinear systems: A flatness-based approach*. Springer Science & Business Media.

Ngwompo, R.F. and Gawthrop, P.J. (1999). Bond graph-based simulation of non-linear inverse systems using physical performance specifications. *Journal of the Franklin Institute*, 336(8), 1225–1247.

Pham, T.H., Prodan, I., Genon-Catalot, D., and Lefèvre, L. (2015). *Port-Hamiltonian model and load balancing for DC-microgrid lift systems*. Ph.D. thesis, LCIS, Grenoble-INP.

Richard, P.Y., Buisson, J., and Cormerais, H. (2002). Analysis of flatness using bond graphs and bicausality. *IFAC Proceedings Volumes*, 35(1), 25–30.

van der Schaft, A., Jeltsema, D., et al. (2014). Port-hamiltonian systems theory: An introductory overview. *Foundations and Trends in Systems and Control*, 1(2-3), 173–378.

Zafeiratou, I., Nguyen, D., Prodan, I., Lefèvre, L., and Piétrac, L. (2018). Flatness-based hierarchical control of a meshed dc microgrid. *IFAC-PapersOnLine*, 51(20), 222–227.